Biosensors and Bioelectronics 100 (2018) 28–34

Contents lists available at ScienceDirect

Biosensors and Bioelectronics

journal homepage: www.elsevier.com/locate/bios

Electrochemiluminescent resonance energy transfer of polymer dots for aptasensing

Feng Sun[a,1], Ziyu Wang[b,1], Yaqiang Feng[a], Yixiang Cheng[b], Huangxian Ju[a,*], Yiwu Quan[b,*]

[a] State Key Laboratory of Analytical Chemistry for Life Science, School of Chemistry and Chemical Engineering, Nanjing University, Nanjing 210023, PR China

[b] MOE Key Laboratory of Mesoscopic Chemistry, School of Chemistry and Chemical Engineering, Nanjing University, Nanjing 210023, PR China

ARTICLE INFO

Keywords:
Polymer dots
Aggregation-induced emission
Electrochemiluminescence
Aptasensor
Lead cation
Signal switch

ABSTRACT

This work designed a three-component polymer for the preparation of polymer dots (Pdots). The polymer contained 9-(diphenylmethylene)-9*H*-fluorene (DPF), 9,9-dioctyl-9*H*-fluorene (DOF) and 1,1′-binaphthyl moieties, and was synthesized via Pd-catalyzed Suzuki reaction. It exhibited obvious yellow-colored aggregation-induced emission (AIE) for fluorescence enhancement at 543 nm via an intramolecular fluorescence resonance energy transfer from DOF moiety to DPF moiety. The Pdots prepared by nanoprecipitation could be conveniently cast on electrode surface and showed a stable anodic electrochemiluminescence (ECL) emission in the presence of triethylamine as a co-reactant. The ECL emission could be effectively quenched by rhodamine B via resonance energy transfer, which led to an "off-on" switch for the design of ECL sensing methodology. Using Pb^{2+} as a target model, an ECL aptasensor for the detection of trace Pb^{2+} was proposed, which showed a linear range of 100 pM to 1.0 μM with a detection limit down to 38.0 pM This work demonstrated the first Pdots prepared with AIE-active polymer for highly efficient ECL sensing.

1. Introduction

Due to the separation of excitation mode from signal detection to produce low background, electrochemiluminescence (ECL) has become a powerful analytical technique with broad range of applications in various areas (Deng and Ju, 2013; Forster, 2009; Hu and Xu, 2010; Zhao et al., 2015). A considerable number of ECL biosensing methods have been developed for the detection of biological small molecules (Li et al., 2012; Liu et al., 2014; Lu et al., 2013; Stewart et al., 2015), nucleic acids (Chen et al., 2015; Feng et al., 2015; Patolsky et al., 2002; Roy et al., 2016), proteins (Han et al., 2014; Jie et al., 2017; Li and cui, 2013), metal ions (Chen et al., 2014; Huang et al., 2015; Li et al., 2015) and so on. To expand the application and improve the luminous properties, great efforts have been devoted to developing novel ECL emitters with low exaction potential, stable and strong emission. These ECL luminophores can be divided into three types: inorganic molecules, organic molecules and semiconductor nanoparticles (quantum dots, QDs) (Miao, 2008). Compared with organic dyes and metal complex emitters, QDs possess specific advantages such as size/surface-trap controlled luminescence and good stability against photobleaching (Bruchez et al., 1998; Michalet et al., 2005). However, semiconductor QDs such as CdTe, PbS, CdS, CdSe and CdSe/ZnS QDs usually contain toxic heavy mental element, which greatly limits their application for bioassay. Thus, developing environmentally friendly and nontoxic ECL emitters is of great significance.

Many non-toxic nanomaterials such as graphite-like carbon nitride (Chen et al., 2013; Cheng et al., 2012), carbon QDs (Zheng et al., 2009; Zhu et al., 2009), silver and gold nanoclusters (Díez et al., 2009; Hesari et al., 2014; Swanick et al., 2012) have been synthesized as ECL emitters for design of ECL sensing strategies. In recent years, luminescent polymer nanoparticles (Pdots) have been developed as a new class of luminescent nanomaterials with fascinating properties, including variety of species, nontoxic feature, excellent photostablity and extraordinary fluorescence (Lim, 2016; Wu and Chiu, 2013). These advantages enable scientists to further explore the possibility of Pdots in ECL emission, including the anodic and cathodic ECL behaviors of poly [2-methoxy-5-(2-ethylhexyloxy)−1,4-phenylenevinylene] conjugated polymer dots (CP-dots) in aqueous system (Dai et al., 2015b), and silole-containing polymer dots (SP-dots) at low excitation potentials (Feng et al., 2016). These works demonstrate that Pdots can be used as excellent ECL luminophors with huge

* Corresponding authors.
E-mail addresses: hxju@nju.edu.cn (H. Ju), quanyiwu@nju.edu.cn (Y. Quan).
[1] These authors contributed equally to this work.

http://dx.doi.org/10.1016/j.bios.2017.08.047
Received 14 May 2017; Received in revised form 4 August 2017; Accepted 21 August 2017
Available online 23 August 2017

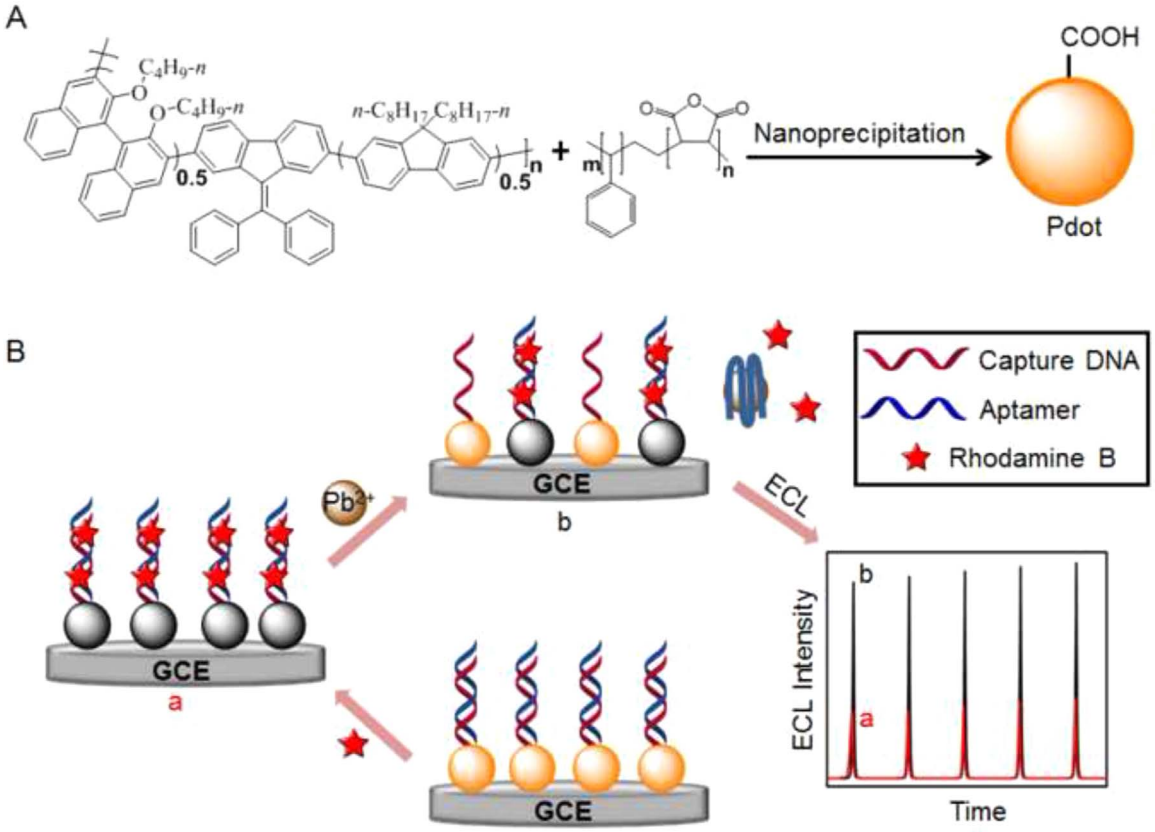

Scheme 1. Schematic diagrams of (A) preparation of Pdots and (B) "off-on" ECL aptasensing for Pb^{2+} detection.

application potential (Chen et al., 2016; Lu et al., 2015; Wu et al., 2016; Zhang et al., 2017). To make use of the aggregation-induced emission (AIE) properties of 9-(diphenylmethylene)–9H-fluorene (DPF), one of the most important AIE monomers (Luo et al., 2011; Mei et al., 2015; Tong et al., 2007), for improving the ECL emission of Pdots, this work designed a three-component polymer containing DPF for the preparation of Pdots (Scheme 1A). The Pdots showed a stable anodic ECL emission in the presence of triethylamine as a co-reactant, which could be quenched by rhodamine B (RhB) via resonance energy transfer from the excited DPF to RhB, leading to the signal switch for the design of ECL sensing methodology.

Based on the ECL quenching of Pdots by RhB, this work further designed an "off-on" switch by the specific recognition of aptamer to its substrate (Scheme 1B). Using Pb^{2+} as a target model, a DNA sequence complementary to the aptamer of Pb^{2+} was firstly bound to Pdots, which could be conveniently cast on electrode surface to capture the aptamer. Upon the interaction of RhB with the formed double-stranded DNA on electrode surface, the ECL emission was quenched, which led to the "off" state. After specific recognition of the aptamer to Pb^{2+}, the aptamer released from the DNA bound Pdots, which led to the leave of RhB from electrode surface and thus produced the "on" state of ECL emission. The ECL aptasensor for Pb^{2+} showed excellent performance with a wide linear range and high sensitivity, demonstrating promising application of the designed Pdots in ECL sensing.

2. Experimental

2.1. Materials and reagents

Tetrahydrofuran (THF, anhydrous, ≥99.9%, inhibitor-free), triethylamine (TEA, ≥99%), benzophenone, 1-bromobutane, 1-bromooctane and fluorene were purchased from Nanjing Chemical Reagent Co., Ltd (Nanjing, China). Trimethyl borate, bromine, *n*-butyllithium, *bis*(pinacolato)diboron, tetrakis(triphenylphosphine)platinum, *p*-toluenesulfonic acid, 1,1′-binaphthol, poly(styrene-*co*-maleic anhydride) (PSMA), RhB, tripropylamine (TPrA), 1-ethyl-3-[3-dimethylaminopropyl]carbodiimide hydrochloride (EDC), 1-hydroxy-2,5-pyrrolidinedione (NHS) and tetrabutylammonium tetrafluoroborate (Bu_4NBF_4) were provided by Sigma-Aldrich Co. Ltd (Shanghai, China). All other reagents were of analytical grade and directly used without further purification. Compound **1** was synthesized with 1,1′-binaphthol and *n*-butyllithium, compound **2** was synthesized with benzophenone and fluorene, **M-1** and **M-2** was synthesized according to our previous work (Zhang et al., 2015; Dai et al., 2015a). Phosphate buffer saline (PBS, 0.1 M) was prepared by mixing stock solutions of NaH_2PO_4 and Na_2HPO_4. Ultrapure water obtained from a Millipore water purification system (≥18 MΩ cm, Milli-Q, Millipore) was used in all assays.

Capture DNA: 5′-NH_2-$(CH_2)_6$-TTTTTTACCCACCCACCC-3′ and aptamer: 5′-GGGTGGGTGGGTGGGT-3′ were ordered from Sangon Bioengineering Co., Ltd (Shanghai, China). DNA stock solutions were prepared with 0.1 M PBS and kept at −4 °C.

2.2. Apparatus

Atomic force microscopic (AFM) image was obtained with an atomic force microscopy (BRUKER Dimension Icon, Germany) with ScanAsyst mode, and the data were processed by NanoScope. The AFM sample was prepared by dropping Pdots aqueous solution onto a freshly torn mica sheet and dried in a desiccator. The transmission electron micrograph (TEM) was obtained using a JEM-2100 TEM instrument (JEOL, Japan), and the sample was prepared by dipping a carbon film in Pdots solution and drying in a desiccator for 3 days to obtain the better dispersion.

Dynamic light scattering (DLS) measurement was performed on a 90Plus particle size analyzer (Brookhaven Instruments Co., USA). The UV–*vis* absorption spectra were obtained by using a Nanodrop-2000C UV–*vis* spectrophotometer (Thermo, USA). Electrochemical experiments were performed on a CHI 660D electrochemical workstation (CHI instruments Inc., China). Electrochemical impedance spectra (EIS) were recorded on an Autolab potentiostat/galvanostat (PGSTAT 30, Eco Chemie B.V., Utrecht, Netherlands) with a three-electrode system in 0.1 M KNO_3 solution containing 5.0 mM $K_3[Fe(CN)_6]/K_4[Fe(CN)_6]$ (1:1) in the frequency range of 0.01 Hz to 100 kHz with an amplitude of 50 mV. Fluorescence measurements were conducted on an F-7000 fluorescence spectrometer (Hitachi Co., Japan) equipped with a xenon lamp. ECL measurements were carried out in a self-made cell on a MPI-E multifunctional electrochemical and chemiluminescent analytical system (Xi'an Remex Analytical Instrument Co., Ltd., China). Ultrasonic synthesis experiments were conducted on the sonicator (Elmasonic P30H, Germany).

2.3. Preparation of three-component polymer and Pdots

The detailed synthesis procedure of the AIE-active three-component polymer (Scheme 1 A and S1), including **M-1**, **M-2** and AIE-active monomer **M-3,** was described in supporting information. The polymer was synthesized via Pd-catalyzed Suzuki reaction of **M-1**, **M-2** and **M-3** at the molar ratios of 1:1:2. The Gel permeation chromatography gave its M_w = 21960, M_n = 7480 and polymer dispersity index = 2.94.

Pdots were prepared in aqueous solution by a nanoprecipitation method according to previous work (Feng et al., 2016). In brief, 20 μg mL^{-1} of polymer stock solution in 2 mL THF was firstly prepared, and quickly added to 10 mL of Milli-Q water in a bath sonicator (120 W, 37 kHz) for 4 min. After THF was removed by rotary evaporation under vacuum, the mixture was filtrated through a 0.22 μm poly(ether sulfones) syringe filter (Millex-GP Filter, Millipore) to obtain pale yellow Pdots dispersion, which could be kept for months without obvious precipitation.

2.4. Preparation of modified electrodes

The glassy carbon electrodes (GCE, 5 mm in diameter) were polished to a mirror using 0.02–0.05 μm alumina slurry (Gaoss Union, Wuhan), and followed by sonication in water, ethanol and water, respectively. After the electrodes were rinsed thoroughly with ultrapure water and dried in N_2 flow, polymer or Pdots modified GCE was prepared by dropping 20 μL polymer THF solution or Pdots aqueous solution (20 μg mL^{-1}) on the surface and dried at room temperature.

The ECL aptasensor was prepared by dropping 20 μL EDC/NHS (10 mM/20 mM) to Pdots modified GCE for 2 h to activate the carboxyl group at room temperature. Afterward, 20 μL of capture DNA (2 μM) was dropped on the electrode, and incubated overnight at 4 °C in a refrigerator, the electrode was washed with PBS and incubated with 20 μL of *n*-hexyl amine (2 mM) for 2 h to block the activated carboxyl group. Finally, 20 μL of aptamer (2 μM) was added to the capture DNA/Pdots/GCE, and incubated in an incubator at 37 °C for 2 h to obtain the aptasensor, which was stored in the refrigerator at 4 °C for further use.

2.5. Electrochemical and ECL measurements

The electrochemical and ECL measurements were performed on electrochemical workstation with the three-electrode system containing the modified electrode as working, a platinum wire as counter, and a Ag/AgCl electrode as the reference electrodes in 3 mL of 0.1 M pH 9.0 PBS containing 0.1 M KNO_3 and 25 mM TEA. The working potential was scanned from 0 to 1.3 or 1.5 V (vs. Ag/AgCl) at a rate of 100 mV s^{-1}, and the voltage of the photomultiplier tube (PMT) was set at 400 V to record the ECL signals.

For target detection, the aptasensor was firstly incubated with 2 mM RhB for 30 min, and then incubated with sample solution for 30 min at room temperature to perform the ECL measurement.

The voltammograms of 9,9-dioctyl-9*H*-fluorene (DOF), DPF and Pdots modified GCE in CH_3CN solution of 0.1 M Bu_4NBF_4 were obtained with a three-electrode system using a platinum wire as counter electrode, and Ag/Ag^+ electrode (0.01 M $AgNO_3$ and 0.1 M Bu_4NBF_4 in CH_3CN) as the reference electrode. Before measurement, the solution was deoxygenated with N_2 for 30 min.

2.6. ECL emission spectrum and efficiency

The ECL emission spectrum was acquired by collecting the light signals at +1.3 V during cyclic voltammetric (CV) scans with a series of long filters (400, 420, 450, 470, 490, 510, 535, 550, 565, 580, 600 and 630 nm) in 0.1 M pH 9.0 PBS containing 0.1 M KNO_3 and 25 mM TEA. The ECL quantum efficiency was calculated using the equation: $\Phi_{ECL} = \Phi^{\circ}_{ECL}(\frac{I}{Q})/(\frac{I^{\circ}}{Q^{\circ}})$, where Φ_{ECL} and Φ°_{ECL} are the ECL efficiency, I and I° are the integrated ECL intensities (integrating ECL spectrum vs. wavelength), and Q and Q° are the consumed charges (integrating voltammetric curve vs. time) of the target and standard control, respectively (Hesari et al., 2014). Herein the ECL spectrum of 1 μM $Ru(bpy)_3^{2+}$ in aqueous solution at +1.2 V with the Φ°_{ECL} value of 1 was used as the reference in 0.1 M pH 9.0 PBS containing 25 mM TPrA and 0.1 M KNO_3. The Φ_{ECL} of Pdots modified on GCE relative to the $Ru(bpy)_3^{2+}$/TPrA system was calculated to be 0.11.

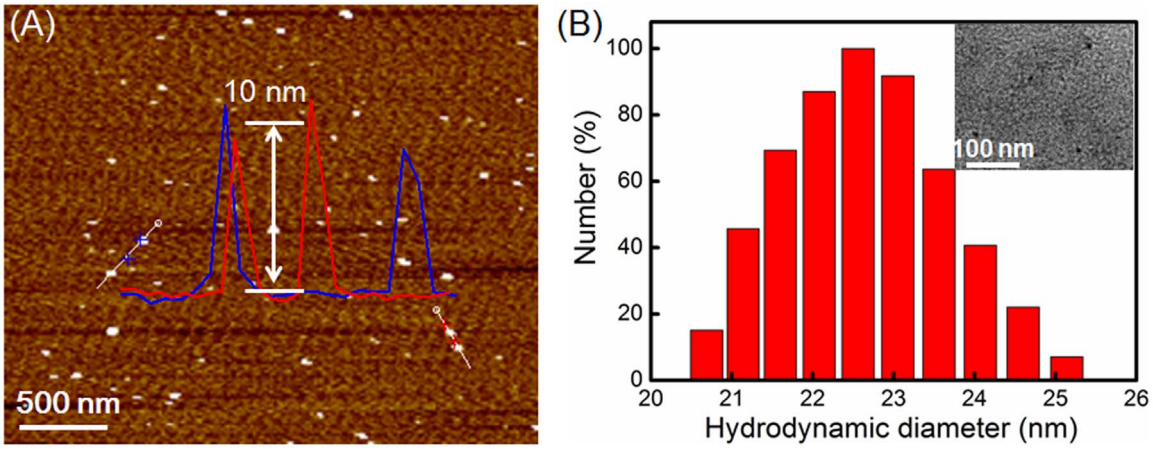

Fig. 1. (A) AFM image and corresponding height of the Pdots on mica sheet. (B) Hydrodynamic diameter of the Pdots measured using DLS. Inset: TEM image of Pdots.

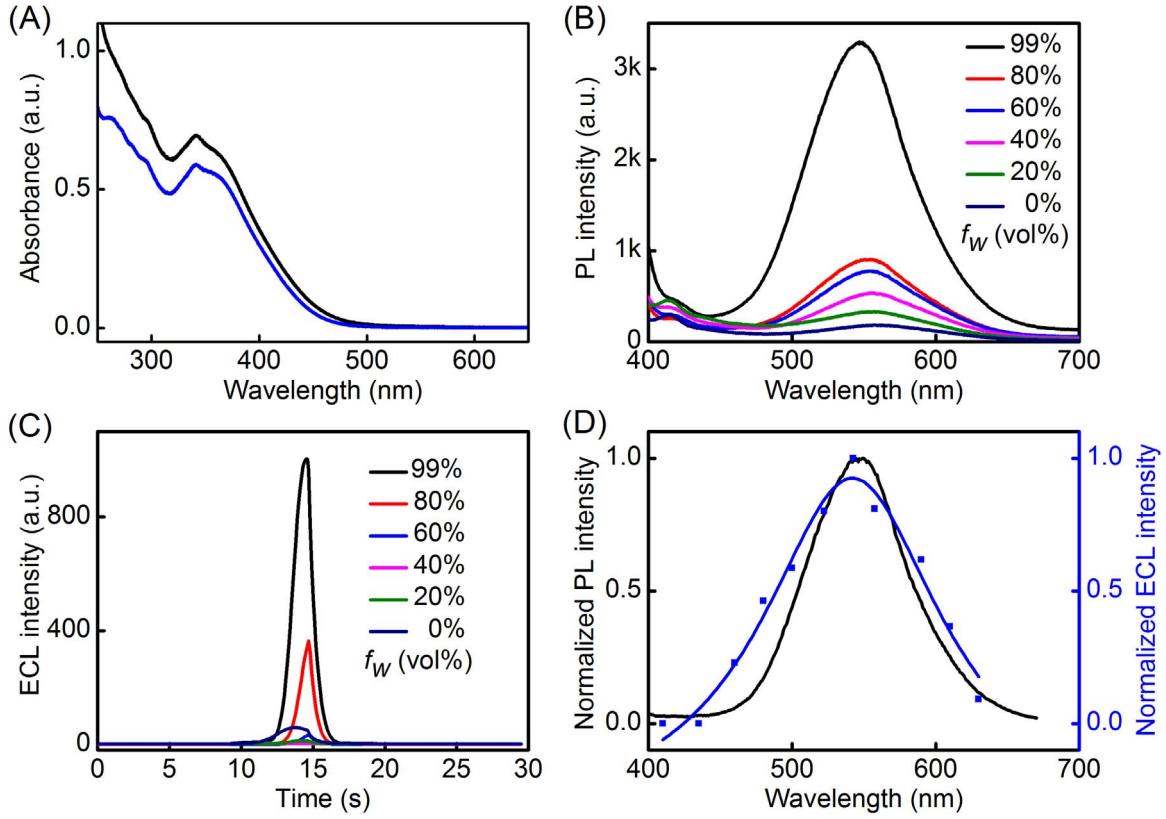

Fig. 2. (A) UV–*vis* absorption of polymer in THF (balck line) and Pdots in water (blue line). (B) Fluorescence spectra of 20 μg mL^{-1} polymer in THF and Pdots formed at different water fractions under 370 nm excitation. (C) ECL-time curves of GCE modified with polymer and corresponding Pdots in 0.1 M pH 9.0 PBS containing 0.1 M KNO_3 and 25 mM TEA at 100 mV s^{-1}. (D) Fluorescence spectrum of Pdots in water (black line) and ECL spectrum of Pdots modified GCE at +1.3 V (blue line).

3. Results and discussion

3.1. Synthesis and characterization of Pdots

Using the polymer as a luminescent precursor and PSMA as the functional group, the carboxylated Pdots were prepared by one-step nanoprecipitation (Scheme 1 A). The AFM image showed the monodisperse properties of the Pdots with a height around 10 nm (Fig. 1A). The TEM image showed the spherical properties and good dispersion of the Pdots on carbon film (Fig. 1B, inset). The hydrodynamic diameter of the Pdots was measured with DLS to be 21–25 nm (Fig. 1B), indicating good hydrophilicity of the Pdots due to the presence of –COOH group.

The UV–*vis* absorption spectra of the polymer in THF and Pdots in water demonstrated the similar absorption peak from 310 nm to 460 nm (Fig. 2A), which was contributed to π–π* transition of the entire conjugated backbone. However, the fluorescence spectra of polymer at various fractions of water (f_w, by volume) showed obvious difference (Fig. 2B). At low fraction of water, the fluorescence spectrum of formed Pdots showed one emission peak at 415 nm and one wide weak emission in 500–600 nm, which were ascribed to the emission from excited DOF and DPF, respectively. With the increasing f_w, the wide emission from DPF showed increased intensity with an emission peak at 543 nm, which was an obvious aggregation induced emission characteristic. Due to the overlap of UV–*vis* absorption of DPF in the Pdots with the fluorescence emission of DOF, the aggregation induced emission of DPF could be described with intramolecular FRET from DOF moiety to DPF moiety (Wang et al., 2017), which also resulted in the increasing ECL intensity of the Pdots formed at increasing volume ratio of water to THF from 40% to 99% (Fig. 2C). At low fraction of water, the irregular change of ECL intensity was owing to the small surface tension of THF, which made the polymer be irregularly stacked on the electrode surface to form local accumulation or aggregation. With the increase of f_w to 20% and then 40%, the water caused larger surface tension, and thus the formed polymer film was more regular. As a result, the ECL intensity rapidly increased to the maximum value as f_w = 99%. This result was consisted with the PL spectrum, indicating that the AIE effect could be responsible for the rapid increase of ECL intensity during the formation of Pdots.

3.2. ECL behavior of Pdots

The Pdots modified electrode did not show any ECL emission at the cathode, even in the presence of H_2O_2 or/and $S_2O_8^{2-}$, the general co-reactant for cathodic ECL emission (Fig. S1). However, strong anodic ECL emission could be observed in the presence of common anodic co-reactants such as TEA and TPrA and a negligible emission in the presence of $H_2C_2O_4$ (Fig. 3A). The anodic ECL intensity increased with increasing concentration of co-reactant, and then reached a maximum at 25 mM TEA (Fig. 3B). The pH value of detection solution also affected the anodic ECL signal of Pdots due to the deprotonation of oxidized TEA or TPrA (Leland et al., 1990; Miao et al., 2002). At the pHs lower than 7.0, the anodic ECL curves showed very little emission. The ECL signal quickly increased with the increase of pH from 7.0 to 9.0 (Fig. 3C). At pH 9.0, the Pdots modified electrode exhibited an excellent ECL reproducibility upon continuous CV scans for 20 cycles (Fig. 3D). This is due to the outstanding film-forming ability of Pdots.

The Pdots modified electrode showed much stronger ECL emission than polymer modified electrode in the presence of 25 mM TEA (Figs. 4A and B). This could be attributed to both the AIE effect and the presence of carboxyl groups on the surface of Pdots. The former resulted in more efficient emission of the excited Pdots, while the latter

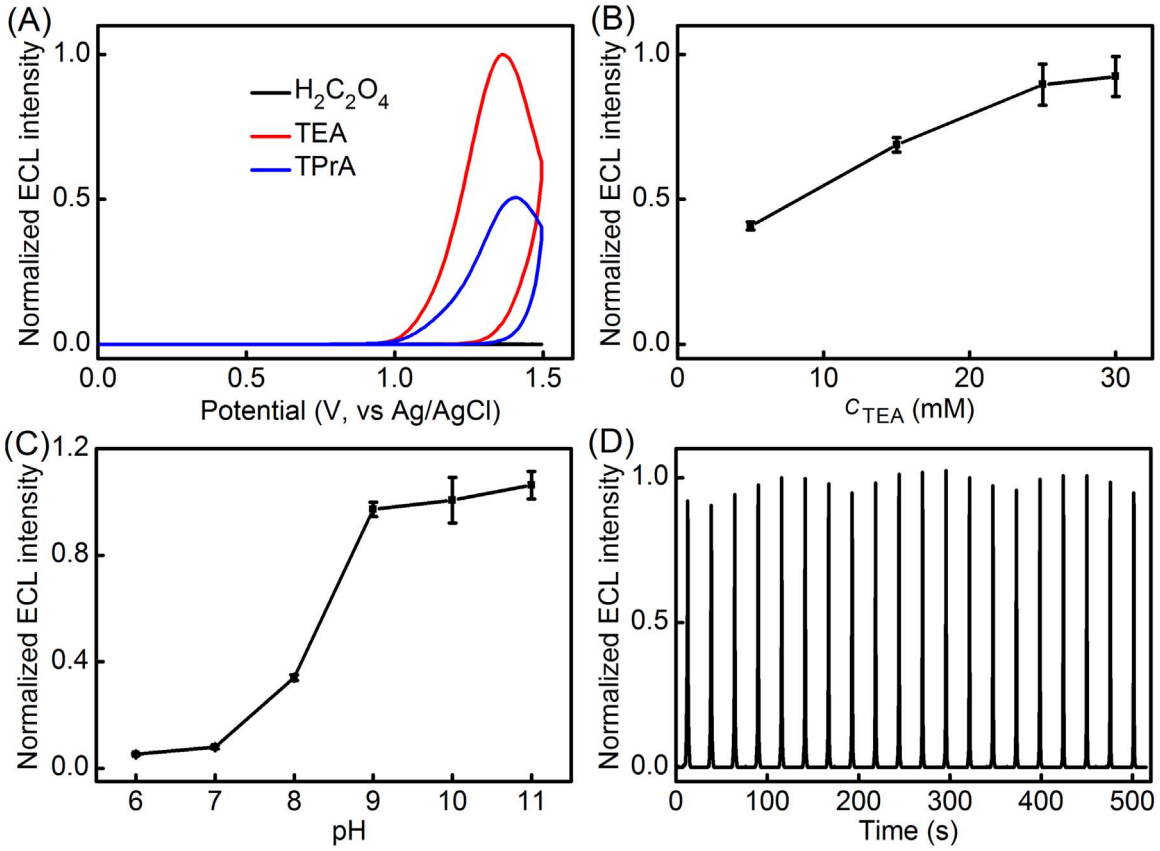

Fig. 3. (A) ECL-potential curves of Pdots modified GCE in 0.1 M pH 9.0 PBS containing 0.1 M KNO_3 and $H_2C_2O_4$ (blank curve), TEA (red curve), or TPrA (blue curve); and effects of (B) TEA concentration, (C) pH and (D) consecutive scan on ECL intensity of Pdots modified GCE. Scan rate: 100 mV s^{-1}.

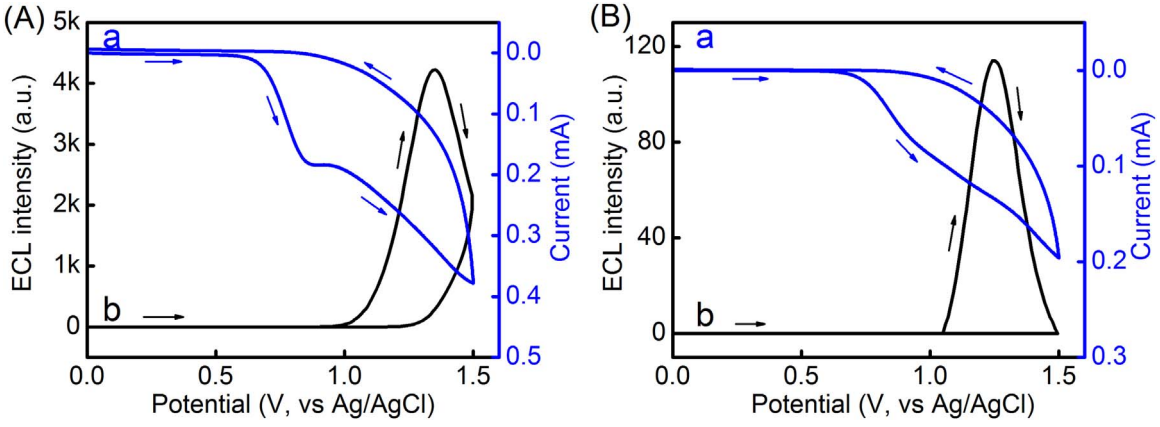

Fig. 4. CV (a) and ECL (b) curves of (A) Pdots and (B) polymer modified GCE in 0.1 M pH 9.0 PBS containing 0.1 M KNO_3 and 25 mM TEA. Scan rate: 100 mV s^{-1}.

made the co-reactant access electrode surface more easily, which led to the formation of more excited Pdots. Thus the oxidation potential of TEA at Pdots modified electrode occurred at +0.82 V, more negative than that of +1.00 V at polymer modified electrode.

3.3. ECL emission mechanism of Pdots modified electrode in the presence of TEA

The CV curve of DOF modified GCE in acetonitrile solution of 0.1 M Bu_4NBF_4 showed two oxidation peaks at + 0.53 and + 0.93 V (vs. Ag/Ag^+), while two oxidation peaks of Pdots modified GCE occurred at +0.63 and +1.03 V (vs. Ag/Ag+) (Fig. S2). Although the Pdots contained three component DOF, DPF and 1,1′-binaphthyl moieties, the modified electrode did not show more oxidation peak. Moreover, the DPF modified electrode was also electrochemically inactive in anodic potential scan from 0 to 1.3 V (Fig. S2). Thus these peaks of Pdots modified GCE could be attributed to the oxidation of DOF moiety. The positive shift of peak potentials resulted from the more stable structure of the polymer. Considering the potential difference of 490 mV between Ag/Ag^+ and Ag/AgCl reference electrodes, the oxidation peak potentials of DOF moiety should be more than + 1.0 V vs Ag/AgCl reference electrode, as observed in Fig. 4.

Interestingly, the ECL spectrum showed the emission peak at 540 nm, which was consisted with the photoluminescence peak of DPF at 543 nm (Fig. 2D), and obviously different from the photoluminescence peak of DOF at 415 nm, indicating that the emission came from the excited DPF. Considering the electrochemical inactivity

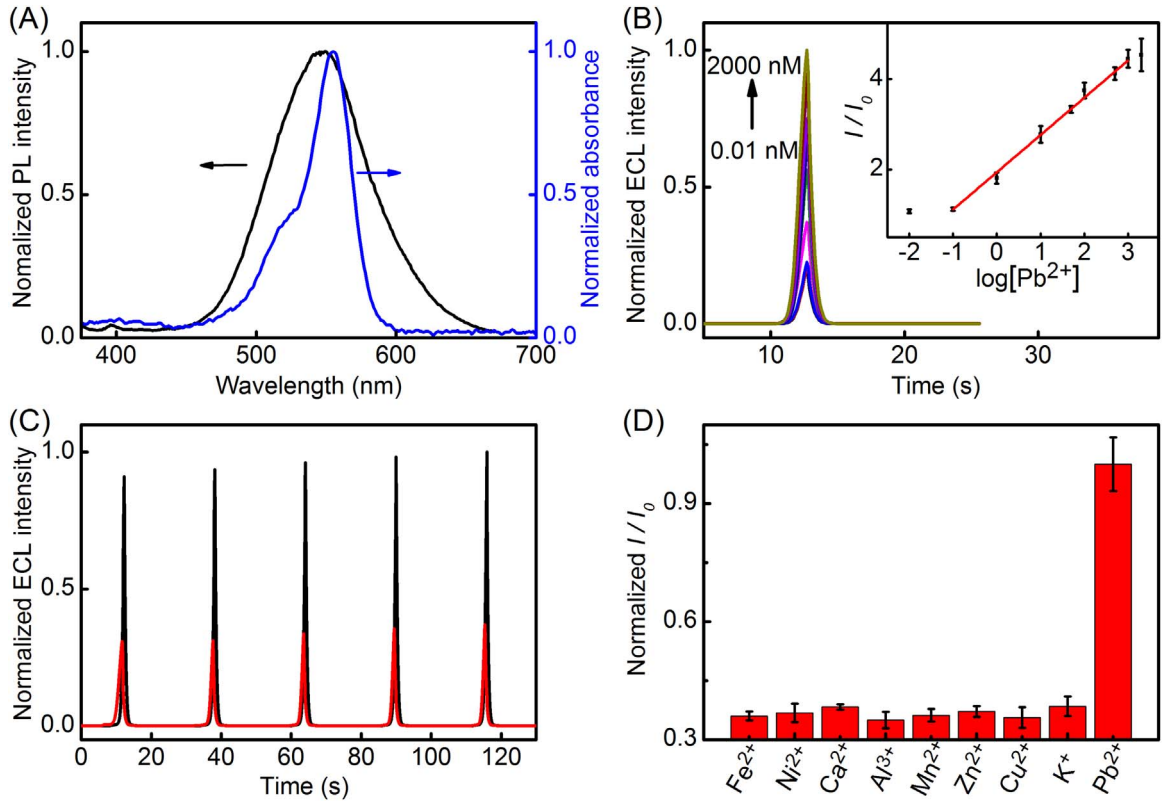

Fig. 5. (A) PL spectrum of Pdots (black) and absorption spectrum of RhB (blue). (B) ECL-time curves of aptasensor in presence of 0.01, 0.1, 1.0, 10, 100, 1000 and 2000 nM Pb^{2+}. Inset: calibration curve (n = 3). (C) Stability of the proposed aptasensor in absence (red) and presence (blank) of 10 nM Pb^{2+}. (D) ECL responses of aptasensor to 1.0 μM Fe^{2+}, Ni^{2+}, Ca^{2+}, Al^{3+}, Mn^{2+}, $Zn^{2+}$and Cu^{2+}, 100 nM K^+ and 10 nM Pb^{2+}.

of DPF and the character of intramolecular FRET from DOF moiety to DPF moiety (Wang et al., 2017), the excited DPF should be formed from the RET from excited DOF to DPF. The excited DOF was produced during anodic scan in the presence of TEA, which led to the formation of $TEAH^{\bullet+}$ and then strongly reductive $TEA^{\bullet}$ (Fig. S3). Thus the ECL mechanism of Pdots modified electrode could be summarized as follows:

$$TEA - e^- \rightarrow TEAH^{\bullet+} \quad (1)$$

$$TEAH^{\bullet+} - H^+ \rightarrow TEA^{\bullet} \quad (2)$$

$$DOF(Pdots) - e^- \rightarrow DOF^{\bullet}(Pdots)^+ \quad (3)$$

$$DOF^{\bullet}(Pdots)^+ + TEA^{\bullet} \rightarrow DOF^*(Pdots) + (C_2H_5)_2NCH = CH_2 \quad (4)$$

$$DOF^*(Pdots) \rightarrow DPF^*(Pdots) \quad (5)$$

$$DPF^*(Pdots) \rightarrow Pdots + h\nu \quad (6)$$

Both the intramolecular RET from excited DOF to DPF and AIE properties of DPF improved the ECL emission of Pdots.

3.4. Feasibility of aptasensor

To investigate the feasibility of the designed aptasensor for Pb^{2+}, the EIS and ECL characters of the modified electrodes during preparation of aptasensor were examined (Fig. S4). After capture DNA was bound to Pdots modified GCE, the electron transfer impedance R_{et} showed obvious increase. The hybridization of capture DNA with aptamer further increased the R_{et}. The adsorption of RhB on the double-stranded DNA led to larger R_{et}. Upon immersion of the RhB/dsDNA/Pdots/GCE in 1 μM Pb^{2+}, the resulting electrode showed a R_{et} value between those of dsDNA/Pdots/GCE and capture DNA/Pdots/GCE (Fig. S4A), indicating the release of some aptamer along with the adsorbed RhB from the electrode surface due to the formation of aptamer-Pb^{2+} complex (Lei et al., 2015). During these treatments, the ECL curves showed opposite change of peak intensity. The Pdots/GCE showed the maximum peak intensity, which slightly decreased upon the binding of capture DNA to Pdots, and then the hybridization of aptamer to capture DNA. After incubating the dsDNA/Pdots/GCE in 2 mM RhB, the ECL emission was quenched (Fig. S4B) due to the binding of RhB to the groove of dsDNA (Islam et al., 2013; Silva et al., 2016). The incomplete quenching of RhB on the ECL of Pdots (curve d in Fig. S4B) resulted from the presence of excessive Pdots, which led to the background signal. The quenching of ECL emission could be attributed to the resonance energy transfer from the excited DPF to RhB, which was demonstrated by the overlapped fluorescence emission of Pdots at 540 nm with the absorption of RhB (Fig. 5A). Thus, after immersing the RhB/dsDNA/Pdots/GCE in 1 μM Pb^{2+} to release the aptamer along with the adsorbed RhB, the ECL emission was recovered, which led to an “off-on” switch for ECL aptasensing for Pb^{2+} detection.

3.5. Pb^{2+} detection

To obtain a high ratio of ECL signal to noise, the detection conditions such as RhB concentration and Pb^{2+} incubation time were firstly optimized to be 2 mM and 30 min (Fig. S5). Under these conditions, the ECL intensity increased with the increasing Pb^{2+} concentration from 0.01 to 2000 nM (Fig. 5B). The plot of I/I_0 vs the logarithm value of Pb^{2+} concentration gave a good linearity in the range of 100 pM to 1.0 μM (R^2 = 0.9955). Here, I_0 and I mean the ECL intensity obtained before and after immersing the RhB adsorbed aptasensor in Pb^{2+} solution, respectively. The limit of detection was 38 pM at a signal-to-noise ratio of 3. The analytical performance was much better than those reported previously (Table S1).

The stability of the Pb^{2+} aptasensor was measured upon continuous CV scan for five circles before and after adding Pb^{2+} (Fig. 5C). The results indicated the acceptable stability in optimized detection conditions. The specificity of the aptasensor was evaluated by immersing the RhB adsorbed aptasensor in the solutions containing 1.0 μM Fe^{2+}, Ni^{2+}, Ca^{2+}, Al^{3+}, Mn^{2+}, Zn^{2+} or Cu^{2+}, or 100 nM K^{+}. Compared with the immersion in 10 nM Pb^{2+}, the ECL recovery upon immersion in these ions was negligible (Fig. 5D), indicating good selectivity of the aptasensor against other environmentally relevant metal ions.

The application of the proposed aptasensor was demonstrated by spiking known amount of Pb^{2+} in two tap water samples. Three determinations of 10 and 100 nM Pb^{2+} gave the RSD of 0.7% and 1.8%, and the average recoveries of 107% and 97.6%, respectively (Table S2), indicating good accuracy of the proposed method for Pb^{2+} detection in the actual samples.

4. Conclusion

A three-component polymer containing AIE-active DPF moiety has been designed for the preparation of Pdots by simple nanoprecipitation of the polymer in aqueous solution. Both the polymer and the Pdots show intramolecular resonance energy transfer from excited DOF moiety to DPF moiety, which leads to improved ECL emission from the DPF moiety due to the ECL resonance energy transfer. The AIE effect of DPF has been demonstrated to be responsible for the increased ECL intensity. The ECL emission can be quenched by RhB via resonance energy transfer from the excited DPF to RhB, which leads to an “off-on” switch for the design of ECL sensing strategy. An aptasensor for Pb^{2+} has been proposed by hybridizing the aptamer with capture DNA/Pdots modified electrode to adsorb RhB, which shows acceptable stability, high sensitivity, wide detection range, excellent selectivity and good accuracy. This work demonstrates the promising ECL sensing application of Pdots with AIE-active moiety.

Acknowledgements

This work was financially supported by National Natural Science Foundation of China (21361162002, 21635005, 21674046, 51673093) and the National Special Project for Key Scientific Apparatus Development (2012YQ170000302).

Appendix A. Supporting information

Supplementary data associated with this article can be found in the online version at doi:10.1016/j.bios.2017.08.047.

References

Bruchez, M., Moronne, M., Gin, P., Weiss, S., Alivisatos, A.P., 1998. Science 281, 2013–2016.
Chen, H.J., Li, W., Wang, Q., Jin, X., Nie, Z., Yao, S.Z., 2014. Electrochim. Acta 86, 94–102.
Chen, H.M., Lu, Q.Y., Liao, J.Y., Yuan, R., Chen, S.H., 2016. Chem. Commun. 52, 7276–7279.
Chen, L.C., Huang, D.J., Ren, S.Y., Dong, T.Q., Chi, Y.W., Chen, G.N., 2013. Nanoscale 5, 225–230.
Chen, Y., Xiang, Y., Yuan, R., Chai, Y.Q., 2015. Nanoscale 7, 981–986.
Cheng, C.M., Huang, Y., Tian, X.Q., Zheng, B.Z., Li, Y., Yuan, H.Y., Xiao, D., Xie, S.P., Choi, M.M., 2012. Anal. Chem. 84, 4754–4759.
Dai, C.H., Yang, D.L., Fu, X., Chen, Q.M., Zhu, C.J., Cheng, Y.X., Wang, L.H., 2015a. Polym. Chem. 6, 5070–5076.
Dai, R.P., Wu, F.M., Xu, H.F., Chi, Y.W., 2015b. ACS Appl. Mater. Interf. 7, 15160–15167.
Deng, S.Y., Ju, H.X., 2013. Analyst 138, 43–61.
Díez, I., Pusa, M., Kulmala, S., Jiang, H., Walther, A., Goldmann, A.S., Müller, A.H.E., Ikkala, O., Ras, R.H.A., 2009. Angew. Chem. Int. Ed. 48, 2122–2125.
Feng, Y.Q., Dai, C.H., Lei, J.P., Ju, H.X., Cheng, Y.X., 2016. Anal. Chem. 88, 845–850.
Feng, Y.Q., Wang, Q.B., Lei, J.P., Ju, H.X., 2015. Biosens. Bioelectron. 73, 7–12.
Forster, R.J., Bertoncello, P., Keyes, T.E., 2009. Annu. Rev. Anal. Chem. 2, 359–385.
Han, F.F., Jiang, H., Fang, D.J., Jiang, D.C., 2014. Anal. Chem. 86, 6896–6902.
Hesari, M., Workentin, M.S., Ding, Z.F., 2014. ACS Nano 8, 8543–8553.
Hu, L.Z., Xu, G.B., 2010. Chem. Soc. Rev. 39, 3275–3304.
Huang, R.F., Liu, H.X., Gai, Q.Q., Liu, G.J., Wei, Z., 2015. Biosens. Bioelectron. 71, 194–199.
Islam, M.M., Chakraborty, M., Pandya, P., Al Masum, A., Gupta, N., Mukhopadhyay, S., 2013. Dye. Pigment 99, 412–422.
Jie, G.F., Tan, L., Zhao, Y., Wang, X.C., 2017. Biosens. Bioelectron. 94, 243–249.
Lei, Y.M., Huang, W.X., Zhao, M., Chai, Y.Q., Yuan, R., Zhuo, Y., 2015. Anal. Chem. 87, 7787–7794.
Leland, K.J., Powell, J.M., 1990. J. Electrochem. Soc. 137, 3127–3131.
Li, F., Cui, H., 2013. Biosens. Bioelectron. 39, 261–267.
Li, M., Kong, Q.K., Bian, Z.Q., Ma, C., Ge, S.G., Zhang, Y., Yu, J.H., Yan, M., 2015. Biosens. Bioelectron. 65, 176–182.
Li, Q., Zheng, J.Y., Yan, Y.L., Zhao, Y.S., Yao, J.N., 2012. Adv. Mater. 24, 4745–4749.
Lim, X.Z., 2016. Nature 531, 26–28.
Liu, Y.T., Lei, J.P., Huang, Y., Ju, H.X., 2014. Anal. Chem. 86, 8735–8741.
Lu, J.J., Yan, M., Ge, L., Ge, S.G., Wang, S.W., Yan, J.X., Yu, J.H., 2013. Biosens. Bioelectron. 47, 271–277.
Lu, Q.Y., Zhang, J.J., Wu, Y.Y., Chen, S.H., 2015. RSC Adv. 5, 63650–63654.
Luo, X.L., Li, J.N., Li, C.H., Heng, L.P., Dong, Y.Q., Liu, Z.P., Bo, Z.S., Tang, B.Z., 2011. Adv. Mater. 23, 3261–3265.
Mei, J., Leung, N.L.C., Kwok, R.T.K., Lam, J.W.Y., Tang, B.Z., 2015. Chem. Rev. 115, 11718–11940.
Miao, W.J., Choi, J.P., Allen, J.B., 2002. J. Am. Chem. Soc. 124, 14478–14485.
Miao, W.J., 2008. Chem. Rev. 108, 2506–2553.
Michalet, X., Pinaud, F.F., Bentolila, L.A., Tsay, J.M., Doose, S.J.J.L., Li, J.J., Weiss, S., 2005. Science 307, 538–544.
Patolsky, F., Katz, E., Willner, I., 2002. Angew. Chem. Int. Ed. 114, 3548–3552.
Roy, S., Wei, S.X., Ying, J.L.Z., Safavieh, M., Ahmed, M.U., 2016. Biosens. Bioelectron. 86, 346–352.
Silva, T.D.S., Castro, A.C.H., Rodovalho, V.R., Madurro, J.M., Madurro, A.J.B., 2016. Solid State Electrochem 20, 2411–2418.
Stewart, A.J., Hendry, J., Dennany, L., 2015. Anal. Chem. 87, 11847–11853.
Swanick, K.N., Hesari, M., Workentin, M.S., Ding, Z.F., 2012. J. Am. Chem. Soc. 134, 15205–15208.
Tong, H., Dong, Y.Q., Hong, Y.N., Häussler, M., Lam, J.W.Y., Sung, H.H.Y., Yu, X.M., Sun, J.X., Williams, I.D., Kwok, H.S., Tang, B.Z., 2007. J. Phys. Chem. C 111, 2287–2294.
Wang, Z.Y., Liu, S.H., Wang, Y.X., Quan, Y.W., Cheng, Y.X., 2017. Macromol. Rapid Commun.. http://dx.doi.org/10.1002/marc.201700150.
Wu, C., Chiu, D.T., 2013. Angew. Chem. Int. Ed. 52, 3086–3109.
Wu, F.M., Feng, Y.Y., Chi, Y.W., 2016. J. Electroanal. Chem. 779, 47–54.
Zhang, S.W., Sheng, Y., Wei, G., Quan, Y.W., Cheng, Y.X., Zhu, C.J., 2015. Polym. Chem. 6, 2416–2422.
Zhang, S.H., Wang, J.M., Zhang, H.Y., Fan, Y.P., Xiao, Y., 2017. Dalton Trans. 46, 410–419.
Zhao, W.W., Wang, J., Zhu, Y.C., Xu, J.J., Chen, H.Y., 2015. Anal. Chem. 87, 9520–9531.
Zheng, L.Y., Chi, Y.W., Dong, Y.Q., Lin, J.P., Wang, B.B., 2009. J. Am. Chem. Soc. 131, 4564–4565.
Zhu, H., Wang, X.L., Li, Y.L., Wang, Z.J., Yang, F., Yang, X.R., 2009. Chem. Commun. 34, 5118–5120.